Journal of Applied Electrochemistry (2021) 51:1157–1174
https://doi.org/10.1007/s10800-021-01564-y

RESEARCH ARTICLE

Structure and corrosion property of pulse electrodeposited nanocrystalline nickel-tungsten-copper alloy coating

Chinmaya Kumar Sarangi[1,2] · Bibhu Prasad Sahu[2] · Barada Kanta Mishra[3] · Rahul Mitra[2]

Received: 1 November 2020 / Accepted: 23 March 2021 / Published online: 11 April 2021

Abstract

Nanocrystalline Ni-W-Cu alloy coatings, synthesized by pulse electrodeposition technique from aqueous sulphate-citrate solution, have been investigated to study the evolved phases, crystallite size, micro-strain, and morphology. The effect of alloying with Cu and its concentration on the corrosion behavior of the Ni-W-Cu coatings in sodium chloride medium was examined through potentiodynamic polarization technique and electrochemical impedance spectroscopy. The increase in the Cu content of the electrodeposited coating improves the crystallinity, leads to grain coarsening, and reduces micro-strain of the Ni-W-Cu alloy coatings. The corrosion resistance is observed to improve because of the formation of Cu_2O-rich barrier film on the Ni-W-Cu alloy surface, which was confirmed through X-ray photoelectron spectroscopy. The addition of Cu is considered as responsible for strengthening the passivation phenomenon and enhancing the oxidation resistance of the Ni-W phase in the coating.

✉ Chinmaya Kumar Sarangi
sarangi.ck@gmail.com

[1] Hydro and Electrometallurgy Department, CSIR-Institute of Minerals and Materials Technology, Bhubaneswar 751 013, India

[2] Metallurgical and Materials Engineering Department, Indian Institute of Technology Kharagpur, Kharagpur 721 302, India

[3] Indian Institute of Technology Goa, Goa 403 401, India

Graphic abstract

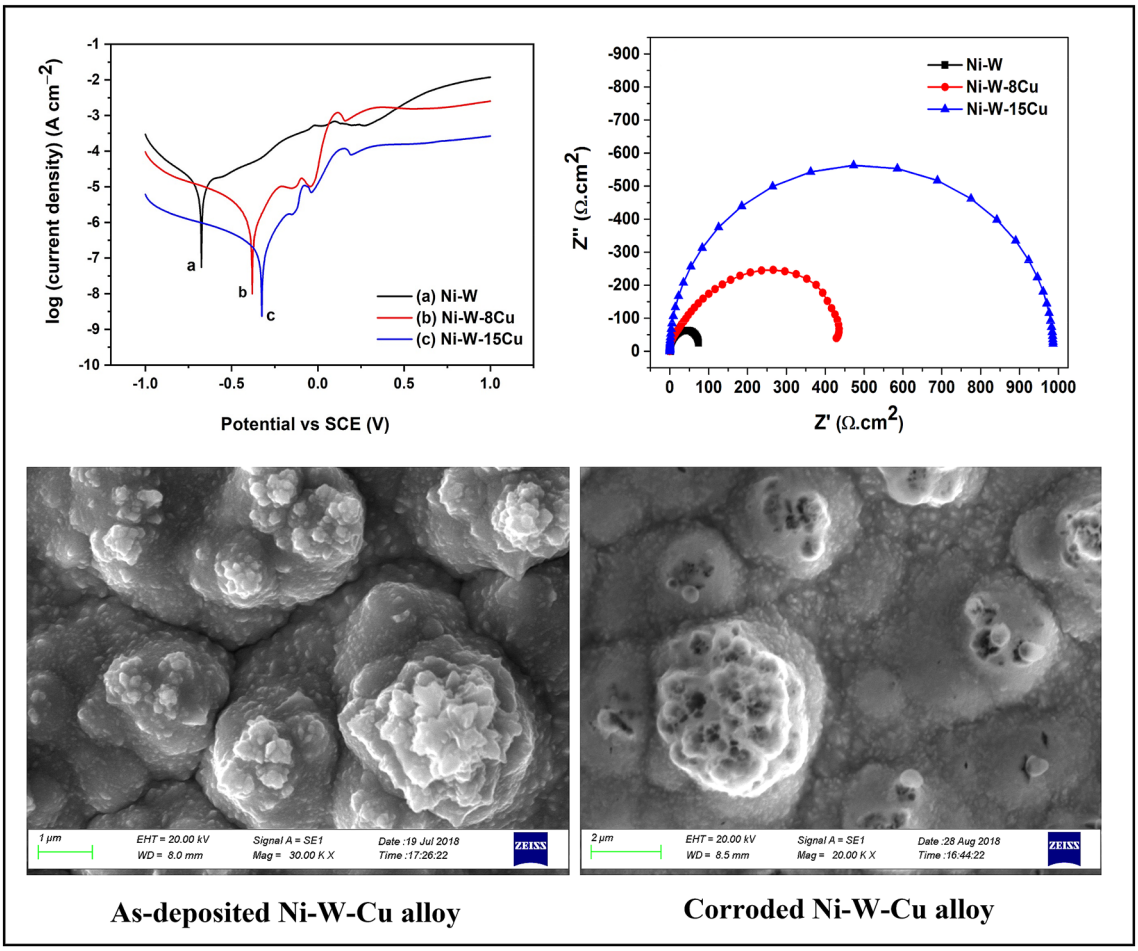

Keywords Ni-W-Cu alloy coating · Pulse electrodeposition · Corrosion resistance · Potentiodynamic polarization · Electrochemical impedance spectroscopy

1 Introduction

Nanocrystalline Ni-W alloy coatings have emerged as an important subject of materials research, because of desirable properties such as mechanical, electrical, magnetic, tribological, and anti-corrosion properties for specific structural or functional applications, and these alloys are also regarded as a promising and favorable substitute for the hazardous hard chromium coatings [1–4]. Particularly, the research on Ni-W binary alloy coatings with W concentration of 5–25 at% has received a considerable attention [5]. Several researchers have confirmed that the passivation current density as well as the corrosion rate in a typical acidic environment can be reduced extensively by raising the W concentration of the Ni-W alloy coating [5, 6]. However, achieving concentrations of W ≥ 25 at% in the alloy is not found to be easy, even if the concentration of tungstate ion is extensively more than the Ni^{2+} ion content in the bath [7]. Furthermore, several researchers have observed that the anti-corrosion performance of the Ni-W alloy coating in sodium chloride medium is affected adversely with the decrease in crystallite size and increase in W content as the WO_3 layer formed on the alloy surface is unstable in neutral or alkaline sodium chloride solution, suggesting that there could be an upper limit of the desirable concentration of W [8, 9]. Therefore, the amount of achievable corrosion resistance property in the binary Ni-W alloys, particularly in sodium chloride environment is probably limited, making it necessary to evolve suitable strategies for ternary alloying of these alloys.

A few literature reports suggest that the corrosion resistance of the parent metal/alloy in different corrosive environments can be improved by alloying with Cu [10–12]. Pardo et al. [13] have stated that the dissolution of metal elements can be hindered by developing a dense

Cu-layer over the surface, which considerably reduces the rate of corrosion of the AISI 304 stainless steel. Hong et al. [14] have also reported analogous explanation for the Cu-containing low alloy steels. Furthermore, several researchers have also found that alloying Ni, Ni–Ti alloy, or stainless steels with Cu increases the corrosion resistance by suppressing the dissolution of the parent metal ions in the corrosive medium through the development of an insoluble salt layer of cuprous or cupric chloride on the surface of the alloy [15–18]. Since most of the aforementioned investigations, devoted to the Cu addition in Ni, Ni-based alloys, or steels, have shown lower corrosion rate for the base metal/alloy [13–18], it would be interesting to study the role of Cu addition to the Ni-W alloy and the evolved structure and corrosion behavior of the Ni-W-Cu ternary alloys. Although very limited research has been carried out on the electrodeposition of such ternary alloys, particularly the optimization of operating conditions and their correlation with composition of the deposited alloy coatings [19, 20], the correlation between structural and corrosion behavior of the Ni-W-Cu alloy coatings has not been studied in detail.

Pulse electrodeposition technique, which is well-accepted as an appropriate technique for the synthesis of nanostructured coatings, is preferred for the production of Ni-W-based alloy coatings [21–25]. Certain advantages such as the ease of controlling process parameters, product purity, and grain size of the deposits, complex shape formation, and high production rate make this technique suitable for industrial applications [26]. Pulse electrodeposition raises the limiting current density by replenishing the metal ions in the diffusion layer during T_{OFF} period [27, 28]. Thus, by applying higher current density during T_{ON} period, alloy coatings with finer grain size (< 30 nm) can be deposited which is not feasible by using direct current electrodeposition technique. It has been observed that pulse electrodeposited coatings possess superior mechanical and corrosion properties as compared to that of direct current electrodeposited coatings [28]. In addition, by modifying pulse deposition parameters, coatings with desired composition, structure, porosity, and hydrogen content can be produced [29].

With this background, the present work has been carried out with the following objectives: (i) to produce nanostructured Ni-W-Cu alloy coatings having varied Cu concentration through pulse electroplating technique from an aqueous sulphate-citrate bath, and (ii) to examine the role of Cu on structure and corrosion resistance of the alloy coatings. For this purpose, an exhaustive study has been conducted on the electrodeposited Ni-W-Cu alloy coatings with specific emphasis on crystallite size, micro-strain, morphology, and corrosion resistance in saline water and the observed behavior has been analyzed by comparing with the base Ni-W alloy coating.

2 Experimental

2.1 Materials and synthesis procedure

The electrolytic bath prepared using analytical grade chemicals and de-ionized water along with the operating conditions employed for pulse electrodeposition of the alloy coatings are listed in Table 1. Prior to the beginning of the electrodeposition process, the electrolytic solution pH was brought to ~ 8.0 using a required quantity of H_2SO_4 or NaOH solution. The temperature of the solution was retained at 75 ± 2 °C by placing it on an automatic-controlled hot-plate. The pulse electrodeposition experiment was conducted by using an electrochemical analyzer (Autolab, Netherlands), while maintaining the conditions as shown in Table 1. The substrate used in the present study was prepared from a Cu sheet with a cathodic dipping area of 1 × 3 cm^2, whereas a Ti sheet coated with Pt was used as the anode. Before each experiment, polishing with different grades of emery paper up to 1200 and cleaning of the substrates were carried out. Subsequently, the area of deposition was activated by treating it with a H_2SO_4 solution of 1 M concentration and then washed thoroughly using distilled water.

2.2 Characterization methods

The electrodeposited alloy coatings were characterized for phase analysis by an X-ray diffractometer (Empyrean PANalytical, Netherland), operated at grazing incidence X-ray diffraction (GIXRD) mode under voltage and current of 40 kV and 30 mA, respectively. While performing the GIXRD scans, the angle between the specimen and incident Cu Kα X-rays of wavelength λ = 1.54 Å was kept at 2°, and the detector was moved at 2° per min with respect to the specimen. For examining the surface morphologies of the coatings and their elemental compositions, a scanning electron

Table 1 Bath composition and process conditions for pulse electrodeposition of the alloy coatings

Composition of bath		Pulse electrodeposition conditions	
$NiSO_4.6H_2O$	0.05 M	Temperature	75 ± 2 °C
$Na_2WO_4.2H_2O$	0.1 M	Bath pH	8.0
$Na_3C_6H_5O_7$	0.5 M	Peak current density	300 mA cm^{-2}
NH_4Cl	0.5 M	Duty cycle	25% (T_{on} 50 ms; T_{off} 150 ms)
$CuSO_4.5H_2O$	0.002 M, 0.004 M and 0.008 M	Stirring rate Deposition time	150 rpm 4 h

microscope (SEM) (Zeiss EVO 18, Oberkochen, Germany) along with an energy dispersive spectroscopy (EDS) attachment (EDAX, Ametek, Draper, Utah, USA) was used.

The potentiodynamic polarization study and electrochemical impedance measurements were performed in 3.5 wt% sodium chloride solution at the ambient temperature using an electrochemical workstation (CH Instruments, Inc. USA) to examine the corrosion behavior of the coatings. The working electrode for the three-electrode corrosion test cell was prepared from the alloy deposit having an exposed area of 1 cm^2; whereas, a saturated calomel electrode (SCE) was used as the reference electrode, and Pt wire worked as the counter electrode. The potential scan rate implemented was 1 mV s^{-1}, while carrying out polarization study for the coatings. The electrochemical impedance spectroscopy was conducted by applying AC maximum potential of 5 mV at frequencies within the range of 1–10^5 Hz. X-ray Photoelectron Spectroscopy (XPS) (PHI 5000 Versa Probe II, Japan) was employed for the analysis of the corroded surfaces of the tested coatings. Before conducting the XPS analysis, Ar^+ sputtering treatment for 60 s was employed to clean the surfaces of the samples, and during the XPS analysis, Al Kα X-rays (1.487 keV) having 100 μm^2 beam size was used.

3 Results and discussion

3.1 Role of copper content in the electrolytic solution

The effect of varying Cu content in the electrolytic solution (125, 250, and 500 mg L^{-1} Cu) has been studied to evaluate the corresponding change in its concentration in the electrodeposited Ni-W-Cu alloy coatings. The concentrations of Ni and W in the deposited Ni-W alloy coating are found to be about ~ 77 at% and ~ 23 at%, respectively, as shown in Fig. 1a. The Cu concentration in the Ni-W-Cu coating is increased from 3 to 15 wt% with rise in the amount of Cu added in the form of $CuSO_4.5H_2O$ in the electrolytic bath, as presented in Fig. 1b-d and Table 2. Since Cu is more electropositive than Ni and W according to the EMF series, the preference for co-deposition of Cu and its concentration in the deposited Ni-W-Cu alloy coatings enhances extensively with the rise in Cu concentration of the electrolytic solution.

3.2 Characterization of electrodeposited alloy coatings

3.2.1 XRD analysis and crystallite size

The comparison of X-ray diffraction patterns of the investigated alloy coatings as shown in Fig. 2 indicates a considerable decrease in peak width with the rise in Cu concentration of the Ni-W-Cu alloy coatings. Moreover, it is noteworthy to mention that the peaks representing {200} and {220} planes, which are not observed in case of the Ni-W alloy coating, become more prominent with their intensities scaling with the Cu concentration of the electrodeposited Ni-W-Cu alloys. In order to examine the possibility of preferred orientation, the texture coefficients have been evaluated using the intensity values of the XRD peaks according to the equation [30]:

$$\text{Texture coefficient } (\%) = \left[I_{\{hkl\}} / \sum \left(I_{\{hkl\}} \right) \right] \times 100 \quad (1)$$

where I is the relative intensity and {h k l} symbolizes different crystal planes represented by the XRD peaks. The presence of only {111} peak is suggestive of < 111 > as the preferred growth direction, whereas the presence of {200} and {220} along with {111} in case of the Cu-containing alloys indicates a decrease in texture coefficient (Table 2). Usually, the predominance of the typical < 111 > texture found in case of the Ni-W alloy is similar to that observed in the fcc-structured films obtained by physical vapour deposition as well [30] and is probably driven by the tendency for lowering of the surface free energy, considering that {111} is the closest packed plane in the fcc structure. The decrease in the texture coefficient of {111} with addition of Cu in the Ni-W-Cu alloy may be ascribed to reduction of surface energy anisotropy for growth along different crystallographic directions.

The crystallite size (d) and micro-strain (ε) of the alloy coatings have been evaluated from the Williamson-Hall relationship [31]:

$$\beta.\cos\theta = k\lambda/d + 4\sin\theta.\varepsilon \quad (2)$$

where θ refers to the Bragg's angle of diffraction, β is the peak broadening, k represents the factor (~ 0.9) related to crystal shape, and λ corresponds to Cu K_α wavelength (1.54 Å). The broadening (β) has been evaluated using the relation:

$$\beta = \sqrt{\left(\beta^2_{\text{sample}} - \beta^2_{\text{standard}} \right)} \quad (3)$$

where β_{sample} and β_{standard} are full width at half maximum (FWHM) of any XRD peak obtained for the alloy deposit sample and the annealed Ni metal sheet, respectively. The FWHM of X-ray diffraction peaks of the annealed Ni was considered as the measure of instrumental broadening. According to Williamson-Hall relation, a graph was plotted by taking 4sinθ and β.cosθ values in the horizontal and vertical axes, respectively (Fig. 3). The size of crystallite and micro-strain of the investigated alloy coatings presented in Table 2 have been calculated from the y-axis intercept and slope of the best-fitline, respectively obtained by the linear

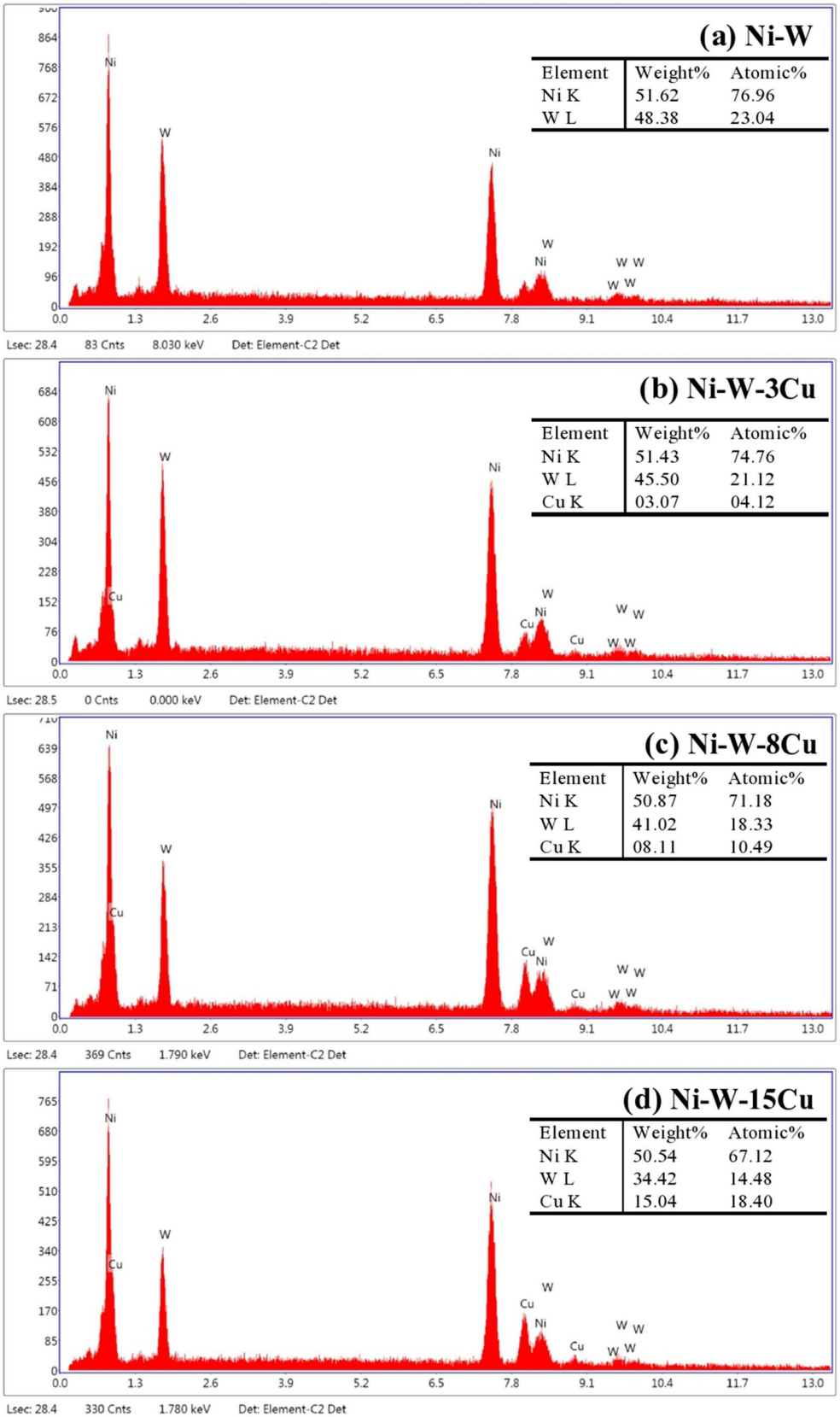

Fig. 1 EDS compositional analysis of the alloys deposited from the baths of varied copper concentrations **a** 0 mg L^{-1} (Ni-W), **b** 125 mg L^{-1} (Ni-W-3Cu), **c** 250 mg L^{-1} (Ni-W-8Cu) and **d** 500 mg L^{-1} (Ni-W-15Cu)

Table 2 Alloy coatings obtained from electrolytic bath with different copper concentrations

Cu concentration in bath (mg L^{-1})	Alloys of different wt% Cu	Crystallite size (nm)	Strain (ε)	Texture coefficient (%)		
				(111)	(200)	(220)
0	Ni-W	14.3	0.0063	100	–	–
125	Ni-W-3Cu	15.1	0.0047	70.3	17.7	12.0
250	Ni-W-8Cu	23.5	0.0035	71.6	17.1	11.3
500	Ni-W-15Cu	29.3	0.0021	70.1	18.4	11.5

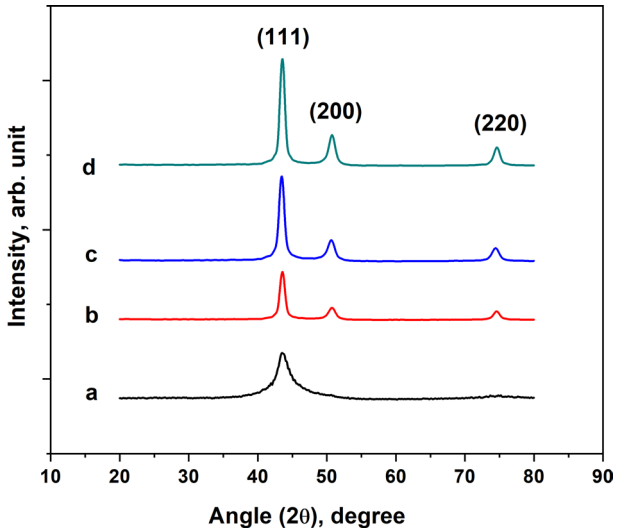

Fig. 2 X-ray diffraction patterns of the alloy coatings with different copper concentrations **a** Ni-W, **b** Ni-W-3Cu, **c** Ni-W-8Cu and **d** Ni-W-15Cu

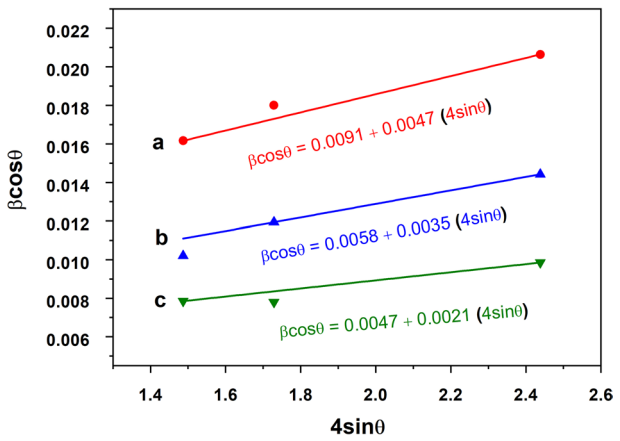

Fig. 3 Evaluation of size of crystallite and strain in the lattice of the alloy coatings **a** Ni-W-3Cu, **b** Ni-W-8Cu and **c** Ni-W-15Cu

regressional analysis of the plot. With rise in Cu concentration of the alloy coatings, the crystallite size is found to increase with the increment being > 2 times on addition of 15 wt% Cu. On the other hand, the micro-strain is observed to reduce with increasing Cu content of the alloy coatings. Both observations with respect to the micro-strain and crystallite size as a result of the increase in Cu concentration of the alloy coatings are consistent with the qualitative observation of the decrease in XRD peak widths (Fig. 2). Therefore, based on the aforementioned observations, it can be inferred that the Cu addition to the Ni-W alloy promotes grain coarsening along with reduction of the micro-strain in the alloy coating. Ghosh et al. [32] have earlier reported a similar phenomenon in case of the Ni-Cu alloy, where an increase in Cu concentration from 26 wt% to 35.8 wt% has resulted in coarsening of the grains by ~ 92% from a size ~ 6.6 nm to ~ 12.7 nm.

3.2.2 Morphological analysis

The morphologies of the investigated alloy coatings have been illustrated in the SEM images as presented in Fig. 4. All the electrodeposited coatings seem to be reasonably well-adhered to the substrate underneath, with absence of any detectable surface microcrack. The microstructure of the Ni-W alloy (Fig. 4a) shows the presence of globular clusters of Ni-W crystallites, and the average size of these clusters increases with Cu addition to the Ni-W alloy, as displayed in Fig. 4b–d. It reveals that alloying with Cu probably contributes to lowering of the nucleation rate, which in turn facilitates grain growth. For the Ni-W-Cu alloy coating, the bright region with cauliflower-like surface morphology as depicted in Fig. 4e and 4f is found to be enriched with Cu whereas the dark region contains relatively less amount of Cu. This observation is also confirmed through EDS mapping of the surface and line profile across the bright and dark regions of the coating (Fig. 5). The EDS map as displayed in Fig. 5a shows the Cu-enriched regions surrounded by Ni-W crystallites, which are distinguished by the significantly populated colour dots of respective elements. The line profile analysis across bright and dark regions of the coating surface as shown in Fig. 5b indicates a prominent rise in the Cu concentration while passing though the white region, followed by reduction in Cu content in dark region, and this observation is in agreement with the inference drawn from the EDS maps. The presence of Cu-rich grains clustered at the centres of globules on the surfaces of Ni-W-Cu alloy coatings, which is represented by green colour dots, is suggestive of

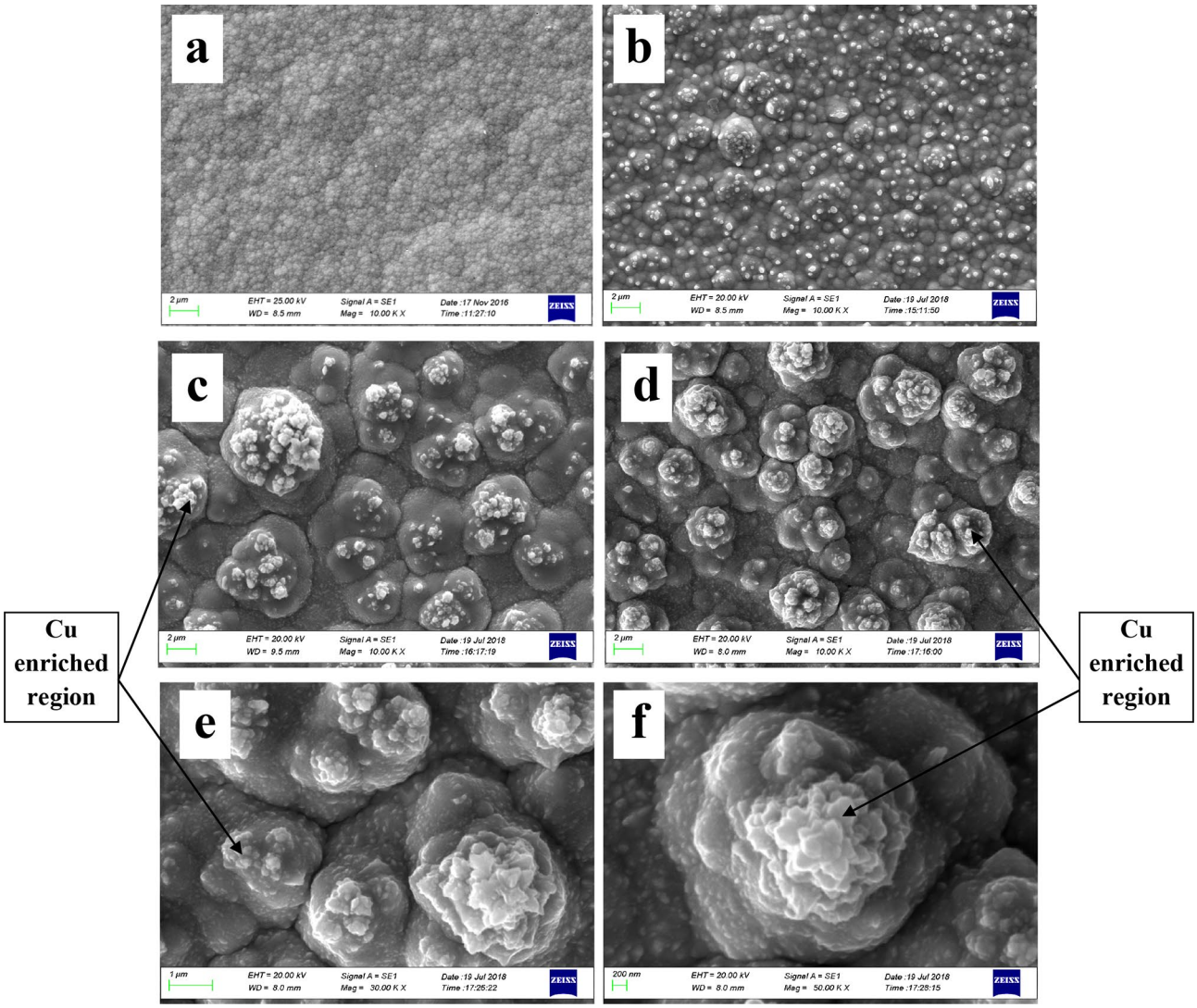

Fig. 4 Morphologies of the alloy coatings with different copper concentrations **a** Ni-W, **b** Ni-W-3Cu, **c** Ni-W-8Cu, **d** Ni-W-15Cu (lower magnification), **e** and **f** Ni-W-15Cu (higher magnification)

segregation or localized enrichment of Cu during growth by electrodeposition. The formation of globular structure at the surface appears to be triggered by the increase in grain size as well as enhanced segregation of Cu with increase in the average Cu concentration of Ni-W-Cu alloy coating, probably because of its limited solubility in the Ni-W alloy and the preferred deposition of Cu-rich grains due to its higher position in the EMF series.

3.3 Potentiodynamic polarization behavior

The corrosion test results evaluated by examining the polarization behavior of the alloy coatings are illustrated in Fig. 6. The Tafel extrapolation method has been employed to determine the corrosion potential (E_{corr}), corrosion current density (i_{corr}), corrosion rate, and resistance to polarization (R_p) for different alloy coatings, and the values of these corrosion test output parameters are presented in Table 3. The polarization curve for Ni-W alloy coating shows the most negative E_{corr} of – 0.675 V and the maximum i_{corr} of ~ 17.86 µA cm^{-2}. With a subsequent increase in the electrode potential above E_{corr}, the anodic current increases gradually and then decreases at 0.1 V, such that an anodic peak current can be identified. Further, a passive layer, formed in between ~ 0.1 and ~ 0.28 V, breaks due to an abrupt rise in current at potential higher than 0.28 V, which is an indication of the active dissolution of the Ni-W alloy coating. Panagopoulos et al. [33] have earlier reported a similar phenomenon for the nanocrystalline Ni-W alloy coating in 0.3 M NaCl medium and mentioned the break-down of a non-protective oxide layer at higher potential values above 0.15 V leading to dissolution of the coating. The outcome of polarization

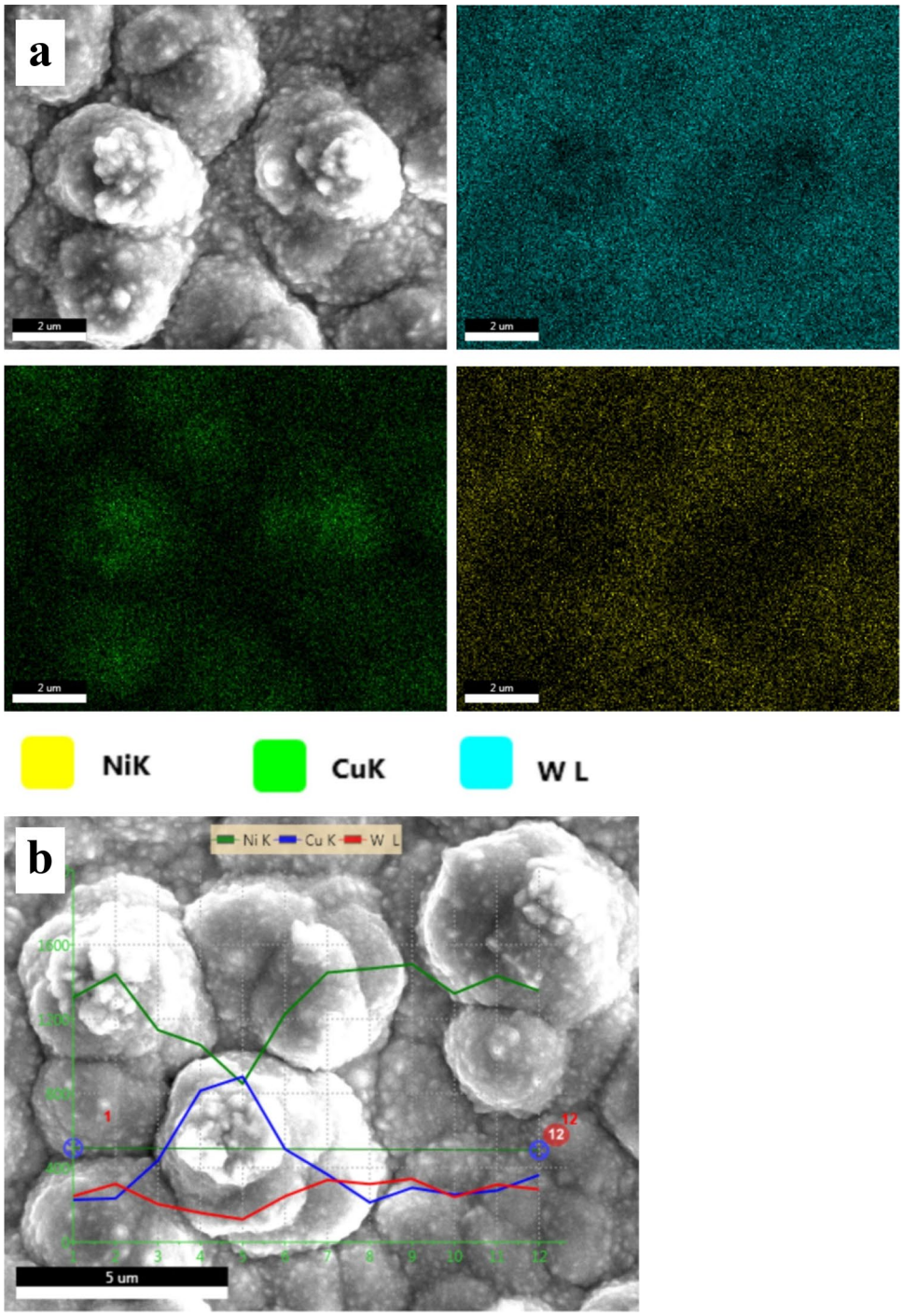

Fig. 5 Identification of Cu-enriched regions of the Ni-W-15Cu alloy coating through **a** EDS mapping and **b** line scan method

study reveals that due to the Cu addition to the Ni-W alloy, i_{corr} decreases, whereas the R_p increases, and as a consequence the E_{corr} shifts towards the more noble direction. It may be noted that the E_{corr} shifts to a more positive value of – 0.38 V, and i_{corr} decreases to ~ 3.51 µA cm^{-2} on addition of 8 wt% Cu. The same trend is followed with further increase in the Cu concentration in the Ni-W-Cu alloy coating to 15 wt% with E_{corr} – 0.321 V and i_{corr} ~ 1.23 µA cm^{-2} such that the Ni-W-15Cu coating is found to exhibit the highest corrosion resistance among the investigated alloy coating samples. The anodic polarization behavior of the Ni-W-8Cu and Ni-W-15Cu coatings (Fig. 6) shows the presence of two distinct active–passive regions, which is not observed in case of Ni-W alloy coating. The existence of wider plateaus of current density representing the polarization behavior of Ni-W-Cu alloy coatings is associated with passivation and subsequent creation of a passive film, which protects from

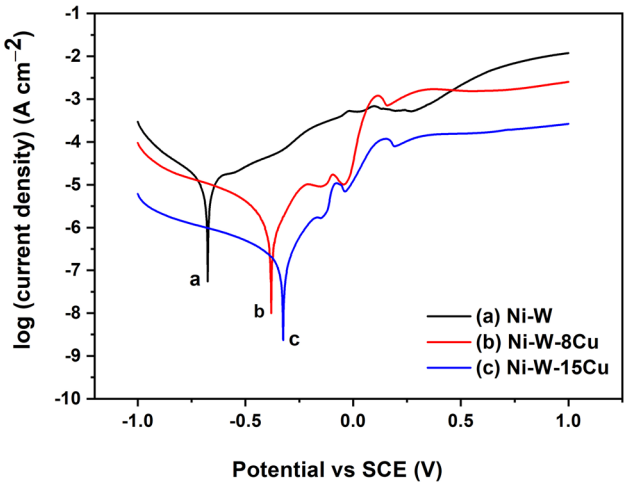

Fig. 6 Potentiodynamic polarization behavior of the alloy coatings with different copper concentrations **a** Ni-W, **b** Ni-W-8Cu and **c** Ni-W-15Cu alloy

further oxidation of the coating and blocks the dissolution of the ternary alloy, resulting in lower corrosion rate.

3.4 EIS measurements

The investigated alloy coatings were also tested for EIS measurements to evaluate their corrosion behavior, and the results have been displayed in the form of Nyquist and Bode plots as shown in Fig. 7a–c. Furthermore, for analyzing the EIS data, an equivalent circuit model shown in Fig. 7d has been used. This circuit model involves the use of the solution resistance (R_s), resistance to charge-transfer (R_{ct}), capacitance of the double-layer (C_{dl}), and a resistor–capacitor combination representing the passive film resistance (R_f) and capacitance (C_f). The Nyquist plots (Fig. 7a) indicate that the Cu addition to the Ni-W alloy has led to higher impedance at all frequencies indicating improved corrosion resistance of Ni-W-Cu alloy coating, which is in agreement with the observations of polarization study. The size of the capacitive semi-circle is also found to increase significantly for the coating with higher Cu content, which appears to have a direct correlation with the corrosion resistance of the Ni-W-Cu alloy.

Bode plots illustrate the variation of modulus of impedance (|Z|) and phase angle (φ) with change in frequency in Fig. 7b and 7c, respectively. At lower frequencies, the modulus of impedance is observed to increase with the rise in Cu content of the coating (Fig. 7b). The Ni-W-15Cu alloy coating exhibits the maximum |Z| value, which indicates that its corrosion rate is lower than Ni-W-8Cu or Ni-W alloy. Moreover, the highest phase angle (φ), displayed by the Ni-W-15Cu alloy coating (Fig. 7c), signifies the existence of a more stable passive film, which results in a higher resistance to the diffusion of Cl^- ions through the coating. It may be noted that the enhanced corrosion resistance because of the presence of Cu as alloying element in the Ni-Cu alloys has been found by several researchers to be related to the increased ionic and electronic resistance of the passive barrier film, which in turn has contributed to the higher modulus of impedance [34–36]. Such a phenomenon has been credited to the inclusion of Ni^{2+} ions in the copper oxide layer that controls the rate of corrosion.

Based on the EIS observations, the equivalent impedance parameters evaluated by means of the circuit model (Fig. 7d) are illustrated in Table 4. The addition of Cu to Ni-W alloy leads to an increase in R_{ct} as well as a reduction in C_{dl} values. The lowering of C_{dl} of the coating is related to the reduction in active area of the coating in contact of the corrosive medium. These observations are in tune with the superior anti-corrosion characteristics of Ni-W-Cu alloy in comparison to the Ni-W alloy and the enhancement of corrosion resistance with rise in the Cu concentration. Furthermore, the trend observed for the passive film resistance (R_f) and capacitance (C_f) values obtained for the investigated Ni-W-Cu alloy coatings are also consistent with their lower corrosion rates due to the formation of a passive layer that efficiently decreases the metal-solution interaction and lowers the transfer rate of Cl^- ions from the corrosive medium. Therefore, it can be inferred that corrosion test outcome, obtained from both polarization behavior and EIS measurements, are in concurrence, and the corrosion rate of the investigated coatings decrease in the following sequence, Ni-W-15Cu < Ni-W-8Cu < Ni-W.

Table 3 Potentiodynamic polarization test parameters for the alloy coatings with varied copper concentration

Type of alloy coating	E_{corr} (V vs SCE)	I_{corr} (μA cm^{-2})	Polarization resistance, R_p (Ω cm^{-2})	Corrosion rate (mil year^{-1})
Ni-W	− 0.675 ± 0.05	17.86 ± 0.09	3274 ± 33	7.578 ± 0.6
Ni-W-8Cu	− 0.380 ± 0.04	3.51 ± 0.06	9557 ± 38	1.629 ± 0.1
Ni-W-15Cu	− 0.321 ± 0.03	1.23 ± 0.02	12,845 ± 46	0.571 ± 0.01

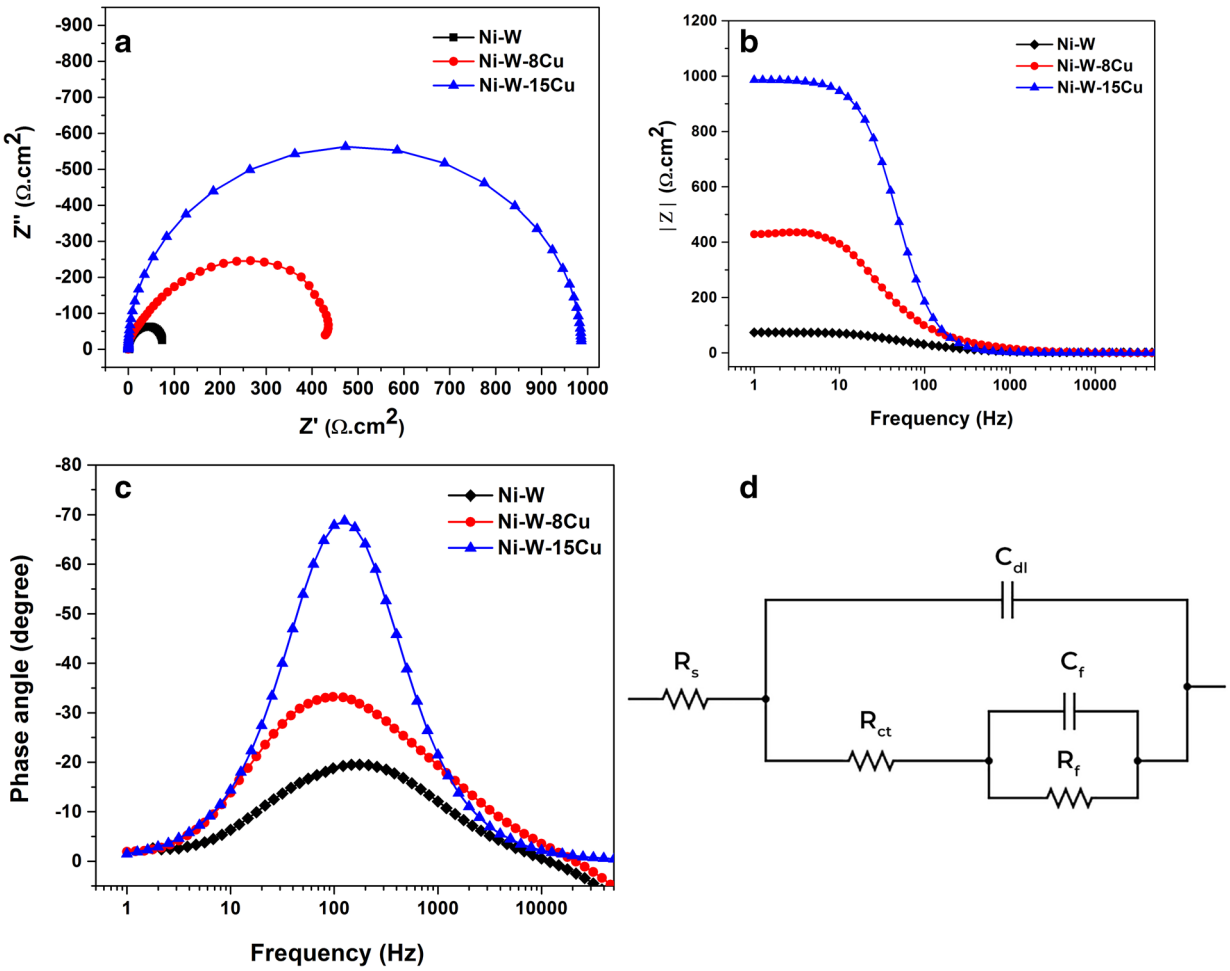

Fig. 7 EIS measurements for the alloy coatings of different copper concentrations **a** Nyquist plot (Z' vs. Z''), **b** Bode plot (Frequency vs. |Z|), **c** Frequency vs. phase angle and **d** Equivalent circuit model employed for fitting the impedance data

Table 4 Electrochemical impedance spectroscopy measurements for the alloy coatings with varied copper concentration derived from Nyquist and Bode plots

Type of alloy coating	R_s (Ω cm^{-2})	R_{ct} (Ω cm^{-2})	R_f (Ω cm^{-2})	C_{dl} (μF cm^{-2})	C_f (μF cm^{-2})
Ni-W	7.8 ± 1.6	73.8 ± 11.4	667.1 ± 25.2	92.6 ± 0.5	4.7 ± 0.2
Ni-W-8Cu	9.2 ± 1.1	428.4 ± 23.5	954.3 ± 17.6	54.1 ± 1.3	3.6 ± 0.4
Ni-W-15Cu	8.4 ± 1.8	986.3 ± 36.8	1544.7 ± 48.5	42.8 ± 0.7	3.2 ± 0.2

3.5 Morphology of the corroded alloy coating surfaces

The top surface and cross-sectional morphologies of the corrosion tested coating samples are displayed in Fig. 8. The corroded surface morphology of the Ni-W alloy coating shows the presence of corrosion pits on the surface, which have grown into elongated pores (Fig. 8a). Examination of the SEM images representing the cross-sectional view of the corrosion tested Ni-W alloy coating shown in Fig. 8b confirms the degree of damage and presence of the elongated pores as a result of growth of the corrosion pits, which is similar to the observation made from the inspection of the top surface morphology (Fig. 8a). However, the damage to the surface through the formation of such corrosion pits is observed to be comparatively less for the investigated Ni-W-Cu alloy coatings,

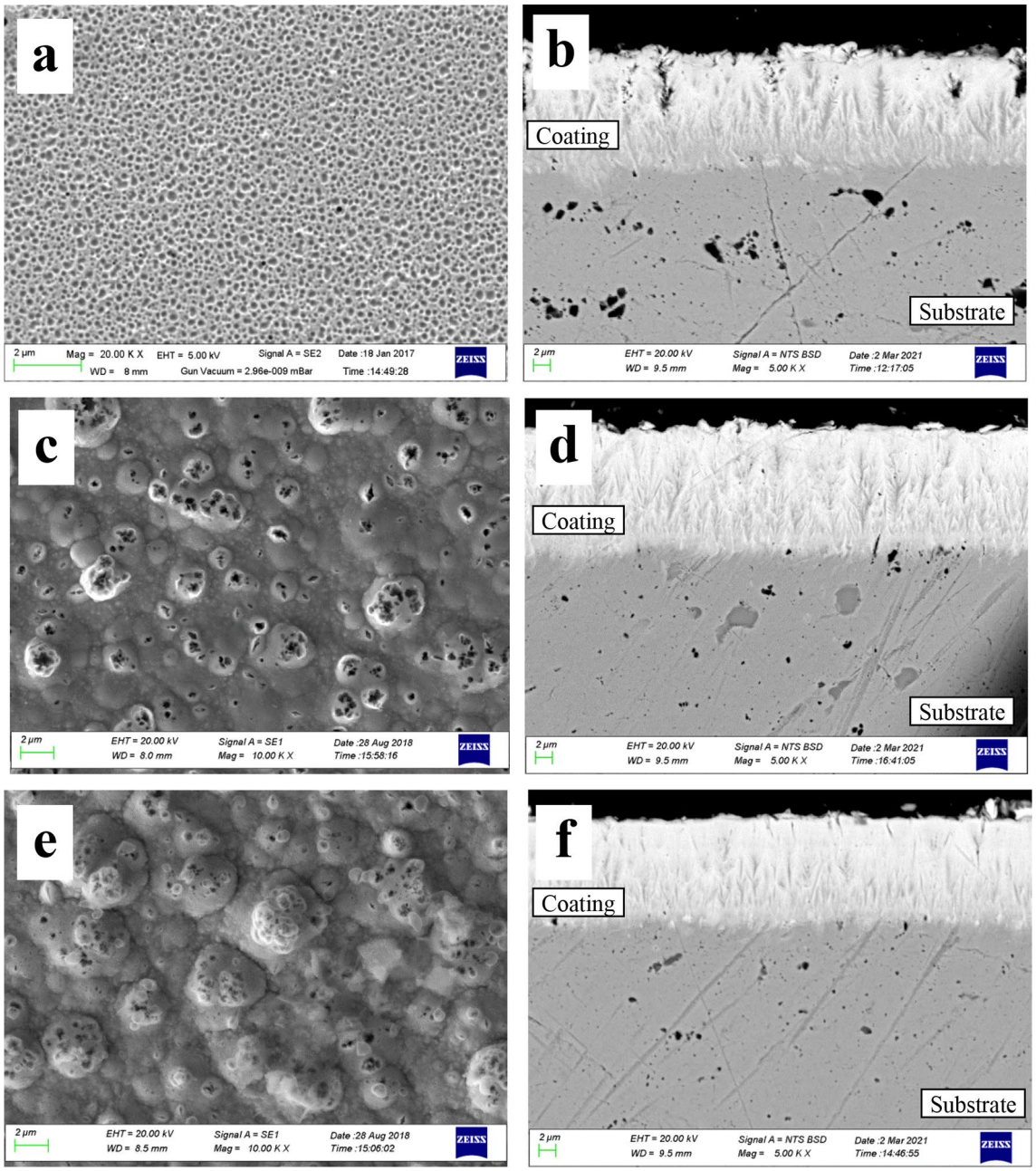

Fig. 8 SEM images of the corrosion tested alloy coatings with different copper concentrations **a** Ni-W (surface), **b** Ni-W (cross-sectional), **c** Ni-W-8Cu (surface), **d** Ni-W-8Cu (cross-sectional), **e** Ni-W-15Cu (surface) and **f** Ni-W-15Cu (cross-sectional)

which is evident from qualitative examination of the corroded surfaces of the Ni-W-8Cu (Fig. 8c) and Ni-W-15Cu coatings (Fig. 8e). With the addition of Cu to the Ni-W alloy, the number of corrosion pits and their growth are found to be reduced, which can be noticed in the cross-sectional images as shown in Fig. 8d and 8f. The corrosion pit size is noticed to progressively shrink with increased Cu concentration of Ni-W-Cu alloys, which can be considered to be in tune with the observations of polarization study and EIS analysis, showing the scaling of corrosion resistance with Cu concentration of the investigated Ni-W-Cu alloy coating.

The EDS maps depicting the distribution of the constituent elements in cross-section of the corroded Ni-W alloy and Ni-W-15Cu alloy coatings are shown in Fig. 9 and Fig. 10, respectively. The EDS maps are collected from the locations shown in the SEM (BSE) images (Fig. 8b and f). Examination of these maps indicates the elemental enrichment of Cu in the corrosion tested Ni-W-15Cu alloy coating.

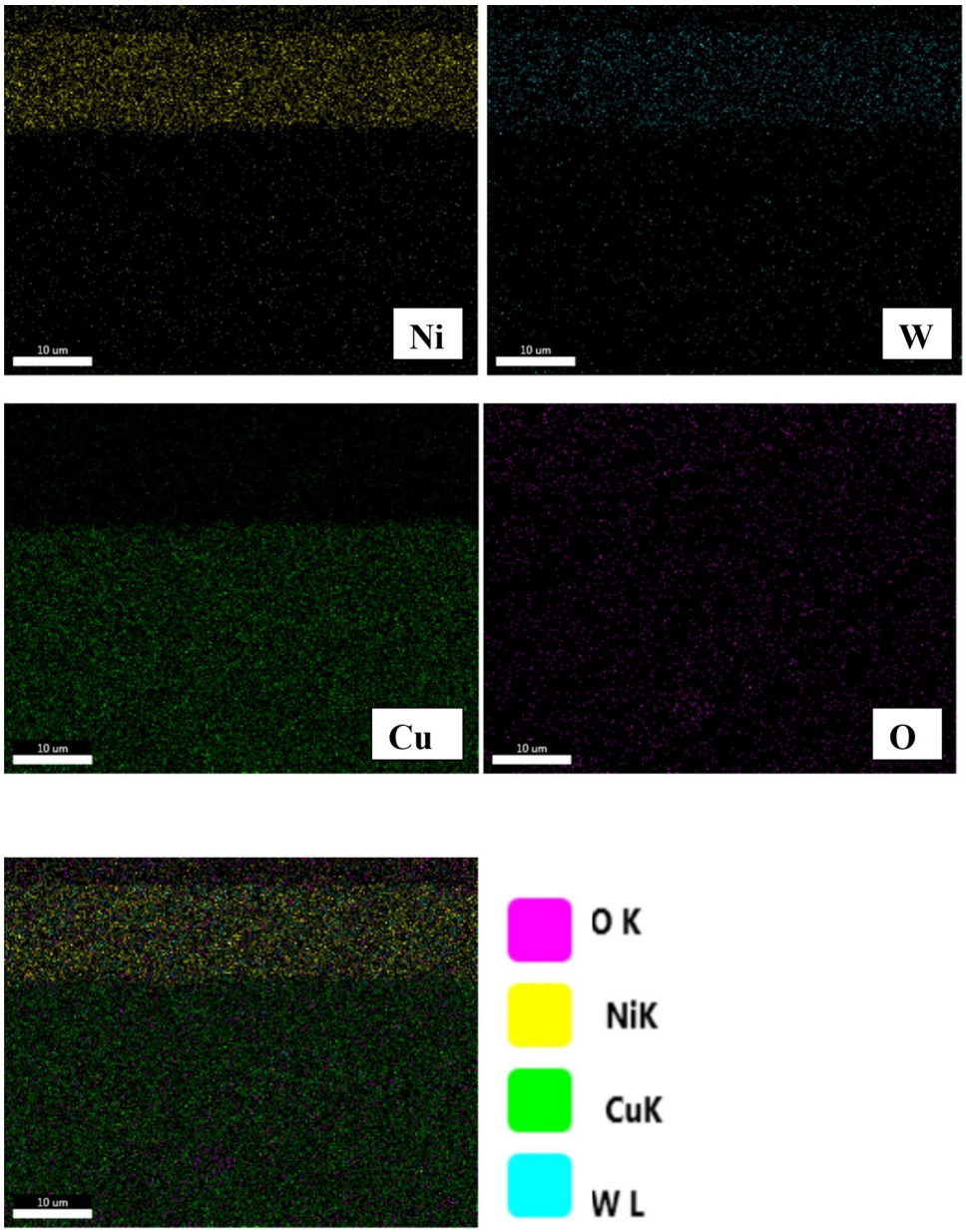

Fig. 9 EDS maps showing the distribution of **a** Ni, **b** W, and **c** O in the cross-section of the corroded Ni-W alloy coating

3.6 X-ray photoelectron spectroscopy of corroded surfaces

For examination of the chemistry of the corrosion tested alloy coating surfaces as well as to understand the mechanism of passivation, the corroded surfaces were investigated by XPS, and the outcome is displayed in Fig. 11. The XPS spectra of Ni-2p with peaks at binding energies of 852.7 eV and 857.9 eV as shown in Fig. 11a reveals the existence of metallic Ni and $Ni(OH)_2$, respectively in the corroded surface of Ni-W alloy coating. In contrast, the XPS peak at the binding energy ~ 855.9 eV as illustrated in Fig. 11b confirms the formation of only NiO on Ni-W-15Cu alloy coating, whereas the peaks representing Ni and $Ni(OH)_2$ are not found, indicating their absence at the corroded surface. The XPS peaks representing Ni and $Ni(OH)_2$ (Fig. 11a) as well as NiO (Fig. 11b) have been matched with the corresponding binding energies, following the available data in the literature [37–39].

The XPS spectrum of Cu-2p obtained from the Ni-W-Cu alloy coating as displayed in Fig. 11c shows two distinct peaks representing Cu and Cu_2O at 932.8 eV and 952.5 eV, respectively. Furthermore, the XPS peaks of O-1 s (Fig. 11d and e) and W-4f (Fig. 11f and g) obtained by Gaussian fitting of the relevant parts of the spectra have been deconvoluted. The O-1 s spectrum collected from the surface film on the Ni-W alloy (as shown in Fig. 11d) exhibits one strong peak at the binding energy of 532.1 eV

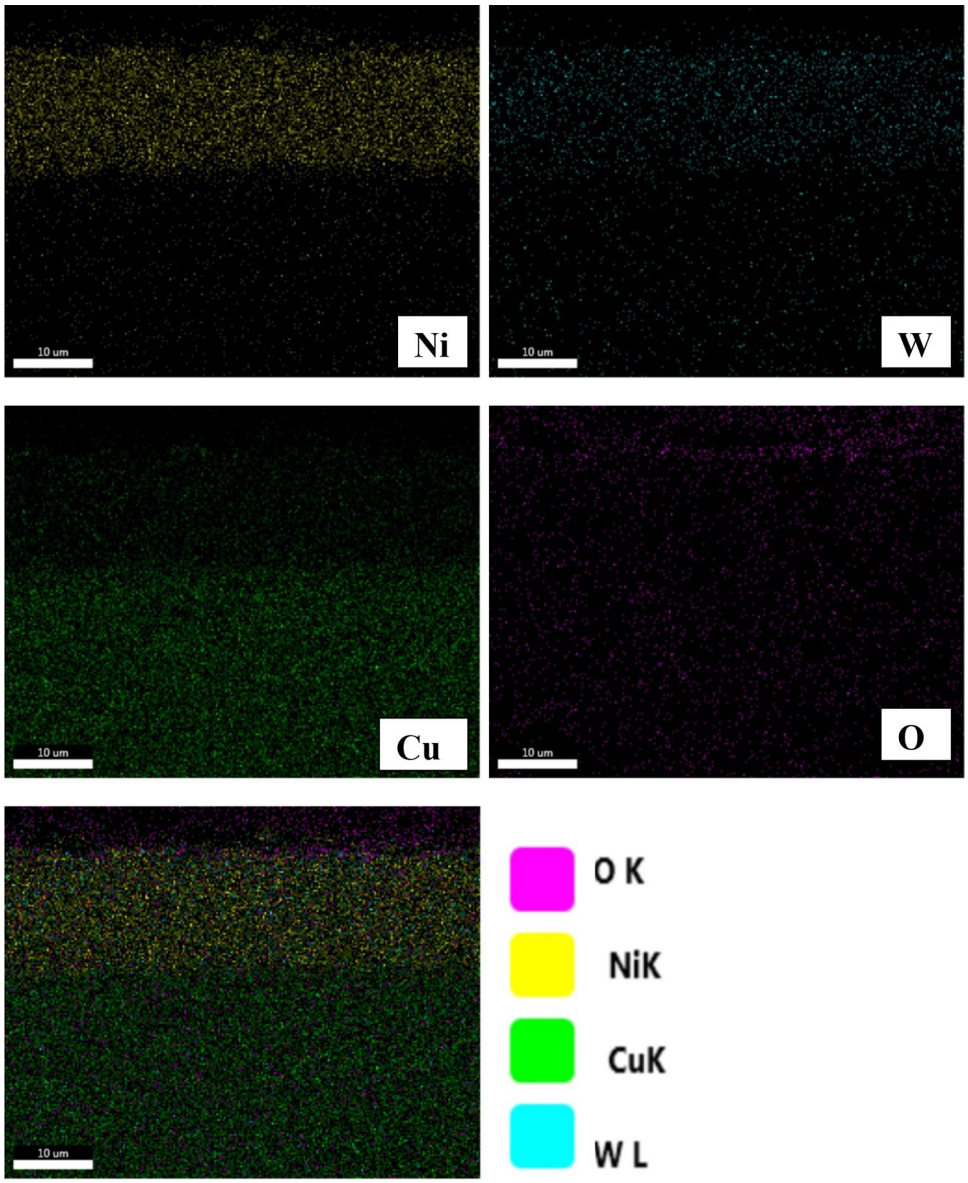

Fig. 10 EDS maps showing the distribution of **a** Ni, **b** W, **c** Cu and **d** O in the cross-section of the corroded Ni-W-15Cu alloy coating

representing OH^-, as well as a relatively weak peak centered at ~ 533.6 eV, which corresponds to $H_2O_{(ads)}$. Furthermore, an XPS peak of O-1 s representing the O^{2-} at the binding energy of ~ 530.1 eV (Fig. 11e) is noticed in case of Ni-W-15Cu alloy coating [39, 40]. This observation also confirms the formation as well as presence of the compounds containing O^{2-} such as NiO and Cu_2O on the corroded surface of the Ni-W-15Cu alloy coating.

The XPS spectra with peaks representing the W-4f from the corroded surface films formed on Ni-W and Ni-W-15Cu alloy coatings are illustrated in Fig. 11f and g, respectively. It is observed that the XPS spectra from both the alloy surfaces consist of a distinct peak representing W centered at ~ 31.4 eV. Moreover, a comparatively weak peak centered at ~ 35.7 eV in the XPS spectrum from the Ni-W-15Cu alloy coating confirms the formation of $NiWO_4$ in tune with the experimental data reported in the literature [8, 23].

3.7 Evolution of corrosion products

In view of the observations of XPS analysis, it is inferred that the possibility of formation of different corrosion products such as $Ni(OH)_2$, NiO, $NiWO_4$, and Cu_2O depends on the constituents of the alloy coating. In case of Ni-W alloy coating, the anodic polarization leads to oxidation of Ni to form $Ni(OH)_2$ on the alloy surface according to the equation [41]:

$$Ni + 2H_2O \rightarrow Ni(OH)_2 + 2H^+ + 2e^- \quad (4)$$

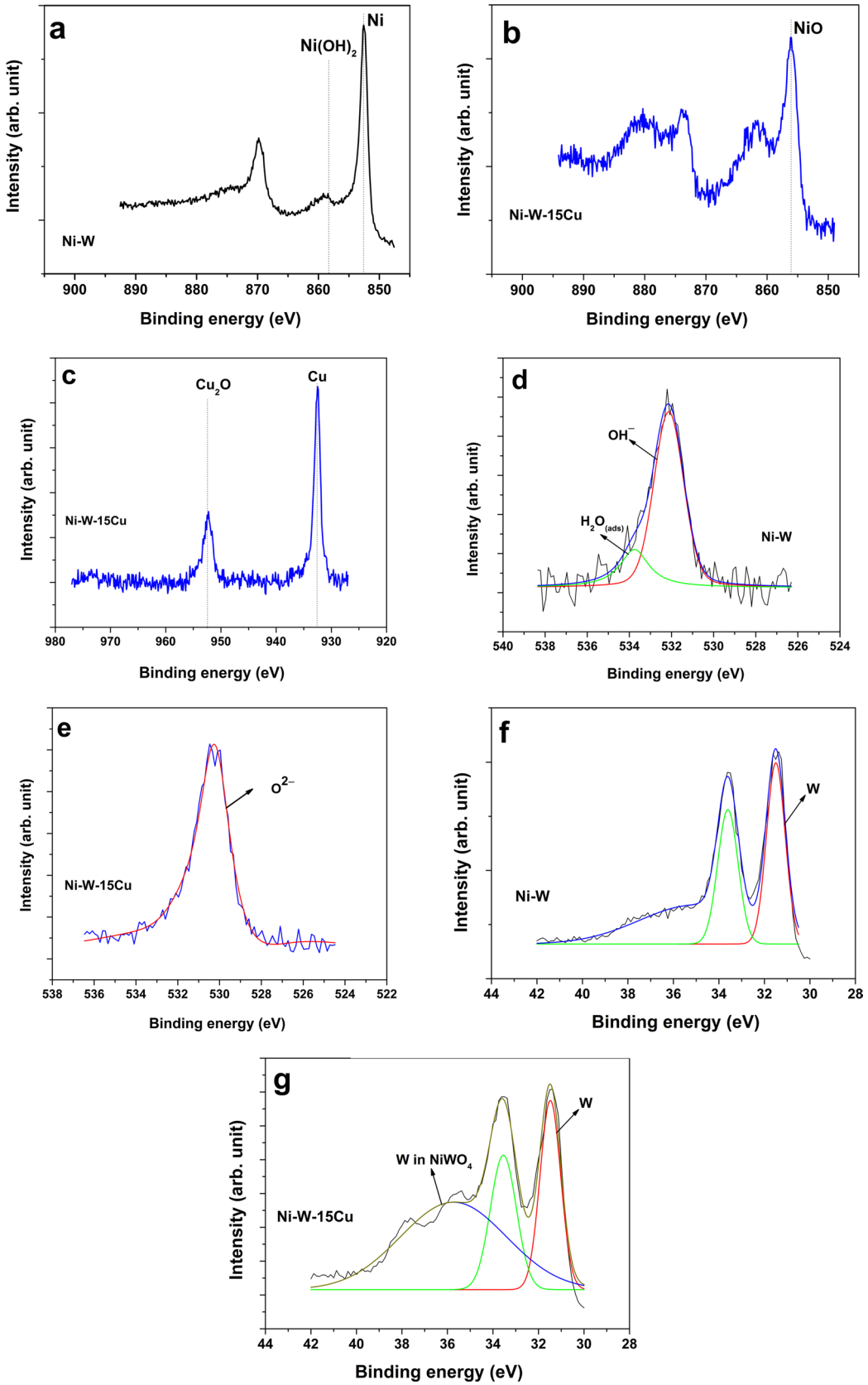

Fig. 11 XPS spectra of corrosion films formed on the surface of the alloy coatings with different copper concentrations **a** Ni-2p (Ni-W), **b** Ni-2p (Ni-W-15Cu), **c** Cu-2p (Ni-W-15Cu), **d** O-1 s (Ni-W), **e** O-1 s (Ni-W-15Cu), **f** W-4f (Ni-W) and **g** W-4f (Ni-W-15Cu)

The passivation behavior exhibited by the Ni-W alloy coating can be ascribed to the formation of $Ni(OH)_2$ on the coating which breaks at anodic potential > 0.28 V (vs SCE), leading to dissolution of the coating. In an earlier study, Onyeachu et al. [39] have reported that the NiO, formed as a passive layer on Ni metal surface, may behave as the preferred site for the adsorption of H_2O and convert to $Ni(OH)_2$ by the reaction:

$$NiO + H_2O \rightarrow NiO.H_2O \rightarrow Ni(OH)_2 \quad (5)$$

However, it is quite interesting to note that such a phenomenon is not observed in case of the Ni-W-15Cu alloy coating as the XPS spectrum from its corroded surface does not show any evidence for the development of $Ni(OH)_2$ and reveals the existence of NiO as the corrosion product (Fig. 11b).

Casciano et al. [41] have reported the possible reaction pathway for the oxidation of W to WO_4^{2-} in the anodic potential regime according to the equation:

$$W + 4H_2O \rightarrow WO_4^{2-} + 8H^+ + 6e \quad (6)$$

The formation of WO_4^{2-} results in the depletion of W from the Ni-W alloy coating and joins the NaCl solution in the form of Na_2WO_4, which is soluble in the aqueous medium. The W-4f peaks in the XPS spectrum from the Ni-W alloy coating (Fig. 11f) does not exhibit any evidence for the presence of WO_3, which further confirms the observation of the oxidation of W to WO_4^{2-} followed by its dissolution in the NaCl solution. However, the XPS spectrum from the Ni-W-15Cu alloy coating as depicted in Fig. 11g indicates the formation of mixed nickel-tungsten oxide ($NiWO_4$), which may have followed the possible reaction pathways for the oxidation of W to WO_2 and subsequent oxidation to form WO_3 according to the Eqs. (7) and (8), probably due to the formation of Cu_2O and NiO as corrosion products instead of $Ni(OH)_2$ that is observed in case of the Ni-W alloy coating.

$$W + 2H_2O \rightarrow WO_2 + 4H^+ + 4e \quad (7)$$

$$WO_2 + H_2O \rightarrow WO_3 + 2H^+ + 2e \quad (8)$$

Benaicha et al. [42] have reported superior anti-corrosion property of Ni-W alloy containing high W concentration because of the creation of a mixed $NiO\text{-}WO_3$ passive film on the coating.

The cathodic reaction occurring on the Ni-W-15Cu alloy coating in contact with the NaCl solution is represented by the oxygen reduction reaction as follows [43]:

$$O_2 + 2H_2O + 4e^- \rightarrow 4OH^- \quad (9)$$

The anodic oxidation reaction in the NaCl solution takes the path of the sequence of preferential dissolution of Cu to generate $CuCl_2^-$ followed by its hydrolysis to form Cu_2O layer on the surface, which can be explained by the reactions as follows [44, 45]:

$$2Cu + 4Cl^- \rightarrow 2CuCl_2^- + 2e^- \quad (10)$$

$$2CuCl_2^- + 2OH^- \rightarrow Cu_2O + H_2O + 4Cl^- \quad (11)$$

3.8 Mechanism of protection

Qualitative examination of the corroded surface of the Ni-W alloy (Fig. 8a and b) as well as the sub-surface locations show the presence of considerable porosity. On the other hand, the corroded surfaces on the Cu-containing alloys exhibit little or no porosity (Fig. 8c–f) whereas the subsurface locations have pores, which are finer in size compared to those in the Ni-W alloy. The results of XPS as shown in Fig. 11b, c and g show the evidence for the formation of Cu_2O in addition to NiO and $NiWO_4$ in the corroded surface film of Ni-W-15Cu alloy. In contrast, the XPS spectra of the corroded surface of the Ni-W alloy show evidence for the formation of $Ni(OH)_2$. The formation of an adherent and protective film on the surface enriched in Cu_2O has restricted the penetration of the Cl^- ions along with the degradation of the underneath alloy. Such mechanism of passivation by formation of the adherent Cu_2O film has been also proposed for the Cu-Ni alloys in an earlier study [46].

As pointed out by the point-defect based theory, the initial pitting reaction occurring at film-solution interface involves the adsorption of Cl^- ions into O^{2-} vacancies [47]. Therefore, to maintain the charge neutrality, an equivalent number of cation vacancies are formed by triggering the process of corrosion involving metal dissolution. In the regime of pitting-susceptibility of austenitic stainless steel, passivation has been achieved by the change in electronic property of the surface film from n-type to p-type [48]. As the Cu_2O is known to be p-type semiconductor with cation vacancies [46], its formation is expected to have a passivating effect by inhibiting the adsorption of Cl^- ions.

The presence of large porosities in the corroded surface film of the Ni-W alloy suggests that the layer of $Ni(OH)_2$, which is known to have a limited passivating effect [39], is ruptured during exposure, permitting further degradation by penetration of Cl^- ions. The XPS profiles obtained from the corroded surface of the Ni-W alloy have not shown any peak of WO_3, which confirms that it is not stable and dissolves in the corrosive medium. It has been reported that W does not form any passive layer in NaCl environment, rather it oxidizes to form tungstate ion (WO_4^{2-}), which combines with $2Na^+$ to form water-soluble Na_2WO_4 [41]. Therefore, the

formation of $NiWO_4$ in the corroded surface of the Ni-W-Cu alloy appears to be possible only due to the formation of a passive layer of Cu_2O. Probably, the formation of a stable ternary oxide, $NiWO_4$ along with Cu_2O, as well as reduced porosity in the surface film has together inhibited the formation of Na_2WO_4. Further, greater stability of $NiWO_4$ or its formation being promoted by the presence of Cu_2O may have inhibited the hydration of NiO to form the relatively more unstable layer of $Ni(OH)_2$ on the corroded surface.

The observation made in this work regarding the corrosion property as a consequence of Cu addition is observed to be in agreement with the results of the earlier studies on addition of Cu in Ni-Co-Cr–Mo, Ni–Al, and Ni–Ti alloys [12, 49, 50]. Yang et al. [12] have reported that on adding 0–4 wt% Cu, the Ni-Co-Cr–Mo alloy exhibits improved corrosion resistance because of the development of a Cu-rich film on the outermost Cr_2O_3 passive layer that has hindered the extensive release of Cr in the corrosive medium. For the Cu-Al-Ni alloy, the incorporation and segregation of Ni^{2+} in the Cu_2O layer has a significant effect in stabilizing the barrier film and lowering the corrosion rate [49]. Iijima et al. [50] have reported that the addition of 5 wt% Cu to the Ni–Ti alloy has shifted the potential by 50–100 mV in the noble direction. In this study, the surface oxide film has been found as mainly composed of TiO_2, with metallic Ni and Cu being concentrated at the coating-oxide layer interface, because of which the release of Ni in the solution is found to be low. Moreover, in a study on the corrosion testing of a typical Ni–Ti-Cu coating, it has been reported by Craciunescu et al. [16] that the presence of Cu as alloying element contributes to the formation of a Cu_2O-rich layer, which decreases the pitting corrosion rate.

Based on the findings of the present study as well as earlier reports, it is well-established that the corrosion resistance of the pulse-electrodeposited Ni-W alloy coating is significantly improved on alloying with Cu. Therefore, it is important to state that the employment of Ni-W-Cu ternary alloy coating in place of Ni-W binary alloy may be a great option for anti-corrosion applications.

4 Conclusions

The structural and anti-corrosion characteristics of the Ni-W and Ni-W-Cu alloy coatings, synthesized by pulse electrodeposition technique, have been studied. The Cu content of the Ni-W-Cu alloy coating is observed to scale with its concentration in the electrolytic solution. The crystallite size of the alloy increases whereas the micro-strain decreases as a result of the increase in Cu content of the alloy. Moreover, because of the rise in Cu content, the Ni-W-Cu alloy coatings show globular clusters of larger size, probably due to bigger crystallite size and segregation of Cu. Corrosion studies involving polarization study and EIS measurements have indicated that the corrosion resistance of Ni-W alloy coating is enhanced with the addition of Cu and increase in its concentration. XPS analysis has revealed the development of a protective Cu-rich oxide barrier film on the Ni-W-Cu alloy coating, which inhibits further coating-solution interaction and hinders the diffusion of Cl^- ions from the corrosive solution, resulting in considerable decline in corrosion rate compared to that observed in case of Ni-W alloy coating. It has been demonstrated in the present study that the alloying addition of Cu in Ni-W alloy coating has a significant effect in modifying both structure and morphology along with improvement of the corrosion resistance.

Acknowledgements The authors are thankful to Prof. S.K. Srivastava, Department of Physics, IIT Kharagpur for facilitating the XPS analysis. The authors would like to acknowledge Ministry of Earth Sciences (MoES), India for providing support to accomplish the present study.

References

1. Bera P, Kumar MD, Anandan C, Shivakumara C (2015) Characterization and microhardness of electrodeposited Ni-W coatings obtained from gluconate bath. Surf Rev Lett 22:1550011–1-1550011–15. https://doi.org/10.1142/S0218625X15500110
2. Zemanova M, Krivosudska M, Chovancova M, Jorik V (2011) Pulse electrodeposition and corrosion properties of Ni-W alloy coatings. J ApplElectrochem 41:1077–1085. https://doi.org/10.1007/s10800-011-0331-y
3. Anicai L (2007) Ni-W alloys coatings as ecological alternative for chromium plating–valuation of corrosion behaviour. Corros Rev 25:607–620. https://doi.org/10.1515/CORRREV.2007.25.5-6.607
4. Alimadadi H, Ahmadi M, Aliofkhazraei M, Younesi SR (2009) Corrosion properties of electrodeposited nanocrystalline and amorphous patterned Ni-W alloy. Mater Des 30:1356–1361. https://doi.org/10.1016/j.matdes.2008.06.036
5. Eliaz N, Sridhar TM, Gileadi E (2005) Synthesis and characterization of nickel tungsten alloys by electrodeposition. Electrochim Acta 50:2893–2904. https://doi.org/10.1016/j.electacta.2004.11.038
6. Yao S, Zhao S, Guo H, Kowaka M (1996) A new amorphous alloy deposit with high corrosion resistance. Corros 52:183–186. https://doi.org/10.5006/1.3292112
7. Metzler OY, Zhu L, Gileadi E (2003) The anomalous codeposition of tungsten in the presence of nickel. Electrochim Acta 48:2551–2562. https://doi.org/10.1016/S0013-4686(03)00297-4
8. Chianpairot A, Lothongkum G, Schuh CA, Boonyongmaneerat Y (2011) Corrosion of nanocrystalline Ni-W alloys in alkaline and acidic 3.5 wt% NaCl solutions. Corros Sci 53:1066–1071. https://doi.org/10.1016/j.corsci.2010.12.001
9. Liu X, Xiang Z, Niu J, Xia K, Yang Y, Yan B, Lu W (2015) The corrosion behaviors of amorphous, nanocrystalline and crystalline Ni-W alloys coating. Int J Electrochem Sci 10:9042–9048
10. Amin MA, Abd El Rehim SS, El-Lithy AS (2010) Corrosion, passivation and breakdown of passivity of Al and Al-Cu alloys in gluconic acid solutions. Electrochim Acta 55:5996–6003. https://doi.org/10.1016/j.electacta.2010.05.055
11. Oguzie EE, Li J, Liu Y, Chen D, Li Y, Yang K, Wang F (2010) The effect of Cu addition on the electrochemical behaviour of stainless steels. Electrochim Acta 55:5028–5035. https://doi.org/10.1016/j.electacta.2010.04.015
12. Yang B, Li J, Gong X, Nie Y, Li Y (2017) Effects of Cu addition on the corrosion behaviour of NiCoCrMo alloys in neutral

chloride solution. RSCAdv 7:40779–40790. https://doi.org/10.1039/C7RA05617F
13. Pardo A, Merino MC, Carboneras M, Viejo F, Arrabal R, Munoz J (2006) Influence of Cu and Sn content in the corrosion of AISI 304 and 316 stainless steels in H_2SO_4. Corros Sci 48:1075–1092. https://doi.org/10.1016/j.corsci.2005.05.002
14. Hong JH, Lee SH, Kim JG, Yoon JB (2012) Corrosion behaviour of copper containing low alloy steels in sulphuric acid. Corros Sci 54:174–182. https://doi.org/10.1016/j.corsci.2011.09.012
15. Silaimani SM, Vivekanandan G, Veeramani P (2015) Nano-nickel-copper alloy deposit for improved corrosion resistance in marine environment. Int J Environ Sci Technol 12:2299–2306. https://doi.org/10.1007/s13762-014-0591-2
16. Craciunescu C, Hamdy AS (2013) The effect of copper alloying element on the corrosion characteristics of Ti-Ni and ternary Ni-Ti-Cu meltspun shape memory alloy ribbons in 0.9% NaCl solution. Int J Electrochem Sci 8:10320–10334
17. Jiangnan Y, Lichang W, Wenhao S (1992) The effect of copper on the anodic dissolution behaviour of austenitic stainless steel in acidic chloride solution. Corros Sci 33:851–859. https://doi.org/10.1016/0010-938X(92)90049-9
18. Xi T, Shahzad MB, Xu D, Sun Z, Zhao J, Yang C, Qi M, Yang K (2017) Effect of copper addition on mechanical properties, corrosion resistance and antibacterial property of 316L stainless steel. Mater Sci Eng C 71:1079–1085. https://doi.org/10.1016/j.msec.2016.11.022
19. Gupta M, Podlaha EJ (2010) Electrodeposition of CuNiW alloys: thin films, nanostructured multilayers and nanowires. J ApplElectrochem 40:1429–1439. https://doi.org/10.1007/s10800-010-0120-z
20. Bacal P, Donten M, Stojek Z (2017) Electrodeposition of high-tungsten W-Ni-Cu alloys. Impact of copper on deposition process and coating structure. Electrochim Acta 241:449–458. https://doi.org/10.1016/j.electacta.2017.05.004
21. Donten M, Cesiulis H, Stojek Z (2000) Electrodeposition and properties of Ni-W, Fe-W and Fe-Ni-W amorphous alloys: A comparative study. Electrochim Acta 45:3389–3396. https://doi.org/10.1016/S0013-4686(00)00437-0
22. Shreeram DD, Li S, Bedekar V, Cong H, Doll GL (2017) Effect of reverse pulse time on electrodeposited Ni-W coatings. Surf Coat Technol 325:386–396. https://doi.org/10.1016/j.surfcoat.2017.06.037
23. Arganaraz MPQ, Ribotta SB, Folquer ME, Benitez G, Rubert A, Gassa LM, Vela ME, Salvarezza RC (2013) The electrochemistry of nanostructured Ni-W alloys. J Solid State Electrochem 17:307–313. https://doi.org/10.1007/s10008-012-1965-3
24. Kumar KA, Kalaignan GP, Muralidharan VS (2012) Pulse electrodeposition and characterization of nano Ni-W alloy deposits. Appl Surf Sci 259:231–237. https://doi.org/10.1016/j.apsusc.2012.07.024
25. Zemanova M, Kurinec R, Jorik V, Kadleclova M (2012) Ni-W alloy coatings deposited from a citrate electrolyte. Chem Pap 66:492–501. https://doi.org/10.2478/s11696-011-0116-0
26. Gurrappa I, Binder L (2008) Electrodeposition of nanostructured coatings and their charactaerization–A review. Sci TechnolAdv Mater. https://doi.org/10.1088/1468-6996/9/4/043001
27. Roy S, Connell A, Ludwig M, Wang N, O'Donnell T, Brunet M, McCloskey P, OMathuna C, Barman A, Hicken RJ, (2004) Pulse reverse plating for integrated magnetics on Si. J MagnMagn Mater 290–291:1524–1527. https://doi.org/10.1016/j.jmmm.2004.11.566
28. Chandrasekar MS, Pushpavanam M (2008) Pulse and pulse reverse plating–Conceptual, advantages and applications. Electrochim Acta 53:3313–3322. https://doi.org/10.1016/j.electacta.2007.11.054
29. Alfantagi AM, Brehaut G, Erb U (1995) The effects of substrate material on the microstructure of pulse-plated Zn-Ni alloys. Surf Coat Technol 89:239–244. https://doi.org/10.1016/S0257-8972(96)02894-0
30. Kumar M, Mishra S, Mitra R (2013) Effect of Ar:N_2 ratio on structure and properties of Ni TiNnanocomposite thin films processed by reactive RF/DC magnetron sputtering. Surf Coat Technol 228:100–114. https://doi.org/10.1016/j.surfcoat.2013.04.014
31. Mote VD, Purushotham Y, Dole BN (2012) Williamson-Hall analysis in estimation of lattice strain in nanometer-sized ZnO particles. J TheorApplPhys 6:6. https://doi.org/10.1186/2251-7235-6-6
32. Ghosh SK, Dey GK, Dusane RO, Grover AK (2006) Improved pitting corrosion behaviour of electrodeposited nanocrystalline Ni-Cu alloys in 3.0 wt% NaCl solution. J Alloys Compd 426:235–243. https://doi.org/10.1016/j.jallcom.2005.12.094
33. Panagopoulos CN, Plainakis GD, Tsoutsouva MG (2015) Corrosion of nanocrystalline Ni-W coated copper. J Surf Engr Mater AdvTechnol 5:65–72. https://doi.org/10.4236/jsemat.2015.52007
34. Blundy RG, Pryor MJ (1972) The potential dependence of reaction product composition on copper-nickel alloys. Corros Sci 12:65–75. https://doi.org/10.1016/S0010-938X(72)90567-7
35. Beccaria AM, Crousier J (1989) Dealloying of Cu-Ni alloys in natural sea water. Br Corros J 24:49–52. https://doi.org/10.1179/000705989798270342
36. Metikos-Hukovic M, Babic R, Skugor I, Grubac Z (2011) Copper-nickel alloys modified with thin surface films: Corrosion behaviour in the presence of chloride ions. Corros Sci 53:347–352. https://doi.org/10.1016/j.corsci.2010.09.041
37. Machet A, Galtayries A, Zanna S, Klein L, Maurice V, Jolivet P, Foucault M, Combrade P, Scott P, Marcus P (2004) XPS and STM study of the growth and structure of passive films in high temperature water on a nickel-base alloy. Electrochim Acta 49:3957–3964. https://doi.org/10.1016/j.electacta.2004.04.032
38. Grden M, Alsabet M, Jerkiewicz G (2012) Surface science and electrochemical analysis of nickel foams. Appl Mater Interfaces 4:3012–3021. https://doi.org/10.1021/am300380m
39. Onyeachu BI, Oguzie EE, Ukaga IC, Njoku DI, Peng X (2017) Ni corrosion product layer during immersion in a 3.5% NaCl solution: Electrochemical and XPS characterization. Port Electrochim Acta 35:127–136. https://doi.org/10.4152/pea.201703127
40. Wu W, Cheng X, Hou H, Liu B, Li X (2018) Insight into the product film formed on Ni-advanced weathering steel in a tropical marine atmosphere. Appl Surf Sci 436:80–89. https://doi.org/10.1016/j.apsusc.2017.12.018
41. Casciano PNS, Benevides RL, de Lima-Neto P, Correia AN (2014) Corrosion resistance of electrodeposited Ni-Mo-W coatings. Int J Electrochem Sci 9:4413–4428
42. Benaicha M, Allam M, Dakhouche A, Hamla M (2016) Electrodeposition and characterization of W-rich NiW alloys from citrate electrolyte. Int J Electrochem Sci 11:7605–7620. https://doi.org/10.20964/2016.09.17
43. Kear G, Barker BD, Stokes K, Walsh FC (2004) Electrochemical corrosion behaviour of 90–10Cu-Ni alloy in chloride-based electrolytes. J ApplElectrochem 34:659–669. https://doi.org/10.1023/B:JACH.0000031164.32520.58
44. Badawy WA, El-Rabiee M, Helal NH, Nady H (2012) The role of Ni in the surface stability of Cu-Al-Ni ternary alloys in sulfate-chloride solutions. Electrochim Acta 71:50–57. https://doi.org/10.1016/j.electacta.2012.03.053
45. Ma AL, Jiang SL, Zheng YG, Ke W (2015) Corrosion product film formed on the 90/10 copper-nickel tube in natural seawater: Composition/structure and formation mechanism. Corros Sci 91:245–261. https://doi.org/10.1016/j.corsci.2014.11.028
46. Jin T, Zhang W, Li N, Liu X, Han L, Dai W (2019) Surface characterization and corrosion behaviour of 90/10 copper-nickel alloy

in marine environment. Materials. https://doi.org/10.3390/ma12111869
47. Macdonald DD (1992) The point defect model for the passive state. J ElectrochemSoc 139:3434–3449. https://doi.org/10.1149/1.2069096
48. Metikos-Hukovic M, Grubac Z, Omanovic S (2013) Change of n-type to p-type conductivity of the semiconductor passive film on N-steel: Enhancement of the pitting corrosion resistance. J Serb Chem Soc 78:2053–2067. https://doi.org/10.2298/JSC131121144M
49. Nady H, El-Rabiei MM (2017) Corrosion behaviour and electrochemical properties of carbon steel, commercial pure titanium, copper and copper-aluminium-nickel alloy in 3.5% sodium chloride containing sulfide ions. Egypt J Pet 26:79–94. https://doi.org/10.1016/j.ejpe.2016.02.008
50. Iijima M, Endo K, Ohno H, Mizoguchi I (1998) Effect of Cr and Cu addition on corrosion behaviour of Ni-Ti alloys. Dent Mater J 17:31–40. https://doi.org/10.4012/dmj.17.31